



**AFRL-RX-WP-TP-2008-4334**

**EFFECT OF STRESS AND STRAIN PATH ON CAVITY  
CLOSURE DURING HOT WORKING OF AN  
ALPHA/BETA TITANIUM ALLOY (PREPRINT)**

**P.D. Nicolaou and S.L. Semiatin**

**Metals Branch**

**Metals, Ceramics, and NDE Division**

**JULY 2007**

**Approved for public release; distribution unlimited.**

*See additional restrictions described on inside pages*

**STINFO COPY**

**AIR FORCE RESEARCH LABORATORY  
MATERIALS AND MANUFACTURING DIRECTORATE  
WRIGHT-PATTERSON AIR FORCE BASE, OH 45433-7750  
AIR FORCE MATERIEL COMMAND  
UNITED STATES AIR FORCE**

REPORT DOCUMENTATION PAGE				Form Approved OMB No. 0704-0188	
<p>The public reporting burden for this collection of information is estimated to average 1 hour per response, including the time for reviewing instructions, searching existing data sources, gathering and maintaining the data needed, and completing and reviewing the collection of information. Send comments regarding this burden estimate or any other aspect of this collection of information, including suggestions for reducing this burden, to Department of Defense, Washington Headquarters Services, Directorate for Information Operations and Reports (0704-0188), 1215 Jefferson Davis Highway, Suite 1204, Arlington, VA 22202-4302. Respondents should be aware that notwithstanding any other provision of law, no person shall be subject to any penalty for failing to comply with a collection of information if it does not display a currently valid OMB control number. <b>PLEASE DO NOT RETURN YOUR FORM TO THE ABOVE ADDRESS.</b></p>					
1. REPORT DATE (DD-MM-YY) July 2007		2. REPORT TYPE Journal Article Preprint		3. DATES COVERED (From - To)	
4. TITLE AND SUBTITLE EFFECT OF STRESS AND STRAIN PATH ON CAVITY CLOSURE DURING HOT WORKING OF AN ALPHA/BETA TITANIUM ALLOY (PREPRINT)				5a. CONTRACT NUMBER In-house	
				5b. GRANT NUMBER	
				5c. PROGRAM ELEMENT NUMBER 62102F	
6. AUTHOR(S) P.D. Nicolaou (El. Venizelou 31) S.L. Semiatin (AFRL/RXLMP)				5d. PROJECT NUMBER 4347	
				5e. TASK NUMBER RG	
				5f. WORK UNIT NUMBER M02R2000	
7. PERFORMING ORGANIZATION NAME(S) AND ADDRESS(ES) El. Venizelou 31 Metals Branch (AFRL/RXLMP) Metals, Ceramics, and NDE Division Materials and Manufacturing Directorate Wright-Patterson Air Force Base, OH 45433-7750 Air Force Materiel Command, United States Air Force				8. PERFORMING ORGANIZATION REPORT NUMBER AFRL-RX-WP-TP-2008-4334	
9. SPONSORING/MONITORING AGENCY NAME(S) AND ADDRESS(ES) Air Force Research Laboratory Materials and Manufacturing Directorate Wright-Patterson Air Force Base, OH 45433-7750 Air Force Materiel Command United States Air Force				10. SPONSORING/MONITORING AGENCY ACRONYM(S) AFRL/RXLMP	
				11. SPONSORING/MONITORING AGENCY REPORT NUMBER(S) AFRL-RX-WP-TP-2008-4334	
12. DISTRIBUTION/AVAILABILITY STATEMENT Approved for public release; distribution unlimited.					
13. SUPPLEMENTARY NOTES Journal article submitted to <i>Metallurgical and Materials Transactions</i> . PAO Case Number: WPAFB 07-1592; Clearance Date: 09 Jul 2007. The U.S. Government is joint author of this work and has the right to use, modify, reproduce, release, perform, display, or disclose the work.					
14. ABSTRACT The effect of strain path and stress state on deformation and cavitation during hot working of Ti-6Al-4V was established via torsion-compression and reversed-torsion tests. Measurements of the cavity area fraction and the size of individual cavities revealed that the rate of cavity closure during the change in strain path following torsion is approximately twice as large in compression compared to reversed torsion. The observations were interpreted in the context of the effect of texture on local stress state and a micromechanical model for the consolidation of porous media. From an engineering standpoint, this work also indicated that the rate of cavity closure decreases with increasing deformation, thus suggesting that very large strains may be required to heal damage totally.					
15. SUBJECT TERMS Ti-6Al-4V, strain, stress, cavity closure, hot working, titanium alloy					
16. SECURITY CLASSIFICATION OF:			17. LIMITATION OF ABSTRACT: SAR	18. NUMBER OF PAGES 36	19a. NAME OF RESPONSIBLE PERSON (Monitor) Sheldon L. Semiatin 19b. TELEPHONE NUMBER (Include Area Code) N/A
a. REPORT Unclassified	b. ABSTRACT Unclassified	c. THIS PAGE Unclassified			

# **EFFECT OF STRESS AND STRAIN PATH ON CAVITY CLOSURE DURING HOT WORKING OF AN ALPHA/BETA TITANIUM ALLOY**

P. D. Nicolaou\* and S.L. Semiatin

Air Force Research Laboratory, Materials and Manufacturing Directorate,  
AFRL/MLLM, Wright-Patterson Air Force Base, OH 45433-7817, USA

\*El. Venizelou 31, 191 00, Megara, GREECE

Tel. +30-229-602 5492, Fax, +30-229-602 5492, e-mail: [NicolaouP@aget.gr](mailto:NicolaouP@aget.gr)

## **ABSTRACT**

The effect of strain path and stress state on deformation and cavitation during hot working of Ti-6Al-4V was established via torsion-compression and reversed-torsion tests. Measurements of the cavity area fraction and the size of individual cavities revealed that the rate of cavity closure during the change in strain path following torsion is approximately twice as large in compression compared to reversed torsion. The observations were interpreted in the context of the effect of texture on local stress state and a micromechanical model for the consolidation of porous media. From an engineering standpoint, this work also indicated that the rate of cavity closure decreases with increasing deformation, thus suggesting that very large strains may be required to heal damage totally.

## **I. INTRODUCTION**

The development of successful manufacturing techniques for metallic materials requires reliable information regarding hot-working characteristics. The proper hot working temperature and deformation rate must be established to produce high quality wrought products of complex geometry. In addition to the avoidance of surface defects that reduce product yield, the control of internal cavitation is also very important because such damage may lead to poor service properties as well as premature failure [1-4].

Because of the industrial significance of damage phenomena, a large amount of research has been conducted to quantify cavitation for various metals and alloys and to develop predictive models. Most of these efforts have focused on the determination of the conditions under which cavitation can be fully suppressed (or at least minimized) or on quantifying cavity-growth kinetics as a function of a stress state. In the latter regard, a number of testing techniques have been employed to investigate cavitation as a function of stress state; these methods include uniaxial tension, biaxial tension, simple shear/torsion, and uniaxial tension with superimposed hydrostatic pressure [4-9]. Because industrial processes such as cogging and open-die forging typically involve complex states of stress and strain, however, increasing attention is now being focused on the effect of strain and strain-rate path on cavitation behavior [10, 11].

The present work is a continuation of earlier efforts on cavitation during monotonic and reversed-torsion testing. The specific objective of the present research was to establish and model the effect of a different strain path (torsion followed by compression) on the closure of cavities and to compare the closure kinetics to those found for reversed torsion. To this end, torsion-compression experiments were conducted on the same material used previously (Ti-6Al-4V with a colony-alpha microstructure), and the results were interpreted using a model originally formulated to treat the consolidation behavior of powder-metal compacts.

## **II. MATERIALS AND PROCEDURES**

### ***A. Material***

The material used in the present work was Ti-6Al-4V which was received in the form of 17.5-mm diameter, hot-rolled bar. The measured chemical composition of the alloy (in weight percent) was 6.25 aluminum, 4.05 vanadium, 0.19 iron, 0.19

oxygen, 0.012 carbon, 0.0004 hydrogen, 0.010 nitrogen, balance titanium; its beta-transus temperature (at which  $\alpha + \beta \rightarrow \beta$ ) was 1000°C. In the as-received condition, the microstructure of the Ti-6Al-4V comprised fine, equiaxed  $\alpha$ . The material was heat treated to develop a colony- $\alpha$  microstructure which is more susceptible to cavitation. This heat treatment consisted of 955°C/30 min + 1040°C/3 min + 815°C/10 min + air cool. Metallographic examination of the heat treated material revealed a microstructure with a prior-beta grain size (and comparable colony size) of ~100  $\mu\text{m}$  and a grain-boundary- $\alpha$  layer approximately 3- $\mu\text{m}$  thick.

The texture of the heat-treated Ti-6Al-4V alloy with the colony microstructure was relatively weak. The principal  $\alpha$ -phase texture components comprised one with the c-axis parallel to the bar axis having an intensity of ~2.2 x random and another characterized by the c-axis tilted ~60° from the bar axis with approximately 1.5 x random intensity. The slight asymmetry of the latter texture component suggested that the bar may have been fabricated using a Turks head mill rather than a conventional bar mill.

#### *B. Torsion-Compression Tests*

To establish the effect of strain-path change on flow response and microstructure/defect evolution, hot working tests comprising torsion followed by uniaxial compression were conducted. Solid-bar specimens for the initial (torsion) testing were machined from the heat-treated Ti-6Al-4V material. Each torsion sample had a gage length of 5.1 mm, and diameter of 8 mm. The complete specimen geometry and a description of the torsion equipment are given in Reference 12.

Torsion-test procedures consisted of preheating and soaking for 10 min at the test temperature, which was 815°C for all experiments, and then twisting to various degrees. The twist rate was selected as such that the effective strain rate at the surface

of the specimen was equal to  $0.04 \text{ s}^{-1}$ . In contrast to previous work [10, 13], only a *forward* twist was applied to each specimen. After the torsional deformation, the specimen was water quenched. Subsequently, a cylindrical, uniaxial-compression sample (whose axis was parallel to the torsion axis) was machined from the gage length. Thus, each compression specimen had a height of 5.1 mm and a diameter of 8 mm.

The test conditions in compression were similar to those used for the torsional prestrain. Specifically, isothermal, hot compression testing consisted of sample/die heating to a test temperature of  $815^{\circ}\text{C}$  using an induction method, soaking at temperature for 10 minutes, hot compression to a 25-pct. height reduction at a constant *axial* true strain rate of  $-0.04 \text{ s}^{-1}$ , followed by forced-air cooling. At the test temperature, the volume fraction of the alpha-phase exceeded 70 pct., which suggests that the flow behavior was dominated by this phase.

Past work [14] showed that extensive cavitation may take place near the outer free surface of cylindrical specimens during *non-isothermal* pancake forging. Such cavitation results from extensive barreling and the associated secondary tensile stresses that are developed at and near the outer diameter. In such instances, finite-element-method (FEM) simulations indicated that the *mean* stress changes from compressive to tensile at a specific imposed axial strain. In the present work, therefore, FEM analysis of the *isothermal*, hot compression test was used in the experimental design to verify that compressive mean-stress conditions were maintained at and near the sample outer diameter during the imposed height reduction of 25 pct.

Torque-twist data obtained from the torsions tests were converted to effective stress-effective strain using standard equations [15]. Similarly, load-stroke data from

the subsequent compression tests were reduced to average pressure-height strain curves by assuming uniform deformation and correcting for the finite stiffness of the test machine.

### *C. Metallographic Analysis*

After torsion and compression testing, a cross section containing the z-r plane of each specimen was prepared for metallographic examination. Standard sample-preparation techniques were utilized; i.e., sectioning using a diamond wheel followed by grinding and final polishing with diamond paste. Cavity sizes and shapes were measured using 200X optical micrographs (taken on as-polished specimens) and the image-analysis software Image J (Version 1.32). For this purpose, scanned micrographs were transformed into pure black- and-white pictures in which each cavity was clearly distinguishable from the fully-dense matrix.

## **III. RESULTS**

The principal results from this work consisted of flow-behavior measurements, FEM estimates of the stress state during the compressive deformation (following torsion), and cavitation observations.

### *A. Flow Curves*

Effective stress-effective strain curves for experiments consisting of torsional pre-deformation of 125° or 225° twist followed by compression to a height reduction of 25 pct. are given in Figure 1. The flow behaviors during reversed-torsion tests are also included. A comparison of the results for the two types of strain paths revealed noticeable differences. For the torsion-reversed torsion tests, for example, strain hardening occurred after the reversal until a peak stress was achieved at a strain increment of ~0.20 from the beginning of the reversed loading. The peak stress did not differ significantly from the stress at the end of the forward-torsion step.

Furthermore, in contrast to the behavior during the forward loading, flow softening was essentially absent during reversed torsion; i.e., the strain-softening exponent  $n$  was less than -0.02. On the other hand, the flow behavior of the material in compression following torsion was very different. A short strain-hardening transient was found during reloading in compression. However, the peak stress was noticeably higher compared to the stress at the end of the first (torsion) step. Secondly, the compression reloading exhibited significant flow softening at a rate comparable to that of the first (torsion) step; i.e.,  $n \sim -0.20$ . A plausible explanation for these observations may lie in the fact that the specimen was not tested immediately after the first step in forward torsion (as was possible with reversed torsion), but was cooled down, machined, and reheated to the test temperature prior to compression. In so doing, the alpha-beta interfaces, which appear to control slip transfer and flow softening [16], may have “healed”, leading to a behavior analogous to that during the initial deformation in torsion.

### B. FEM Results

The continuum FEM analysis was useful in quantifying the stress state as a function of effective strain during hot compression (Figure 2); i.e., the axial, radial, and hoop principal stresses ( $\sigma_z$ ,  $\sigma_r$ , and  $\sigma_\theta$ , respectively) and the mean stress ( $\sigma_M$ ). The results in Figure 2 correspond to a material element lying at the outer diameter/mid-height location of the compression sample, which would have undergone the largest strain during the first deformation step in torsion. The FEM results indicate that  $\sigma_M$  remained negative (compressive) throughout the compression step, thus promoting the closure of cavities.

### C. Cavitation

The cavitation behavior during monotonic torsion has been described previously [12] and hence will be used as a baseline in interpreting the effect of strain path on cavitation during subsequent compression or reversed torsion.

Optical micrographs showed that the extent of cavitation decreased by reversing the torsion direction or by imposing a subsequent compressive strain. An example of this trend is shown in Figures 3a and 3b for initial torsional twists of 125° (effective strain = 0.99) or 225° (effective strain = 1.78), respectively. In each case, the micrographs show the extent of cavitation after forward torsion and after subsequent reversed torsion or compression. From a qualitative standpoint, it is evident that small levels of compression were more effective in closing cavities than relatively larger reversed-torsion strains. These trends were quantified by measurements of the cavity area-fraction  $C_A$  (Figure 4). The value of  $C_A$  at zero strain represents the level of cavitation after the forward torsional prestrain in each case.

Because the cavity area fractions (Figure 4) were small, additional quantitative insight was obtained from the sizes of the 30 largest individual cavities for samples subjected to forward torsion alone, forward + reversed torsion, and forward torsion + compression (Figure 5). The size of each cavity was quantified by an equivalent radius,  $r_{eq}$  derived from the cavity area ( $A_{cav}$ ), measured using image analysis, according to the relation  $r_{eq} = \sqrt{A_{cav}/\pi}$ . The plots in Figure 5 indicate some large cavities were still present after reversed torsion although the overall extent of cavitation was reduced. On the other hand, the compressive deformation significantly reduced the number and size of the largest cavities, a finding of particular importance with respect to durability in subsequent service.

Last, the *reduction* in cavity size during reversed torsion or compression was quantified as a function of the initial cavity size developed during the forward torsion prestrain (Figure 6). To reduce statistical fluctuations, cavity sizes were first collected into groups of five and averaged prior to the comparison; i.e., the five largest cavities were in the first group, the next five largest were in the second group, and so on. The results in Figure 6 clearly indicate that larger cavities closed at a faster rate compared to smaller ones, and the closure rate during compression was significantly faster than that during reversed torsion.

#### IV. DISCUSSION

As has been noted previously [10, 12, 17], cavity growth and closure in anisotropic materials such as Ti-6Al-4V depend on the local stresses developed within grains/colonies. In this regard, the stress ratio (the ratio of the mean to the effective stress) is especially important. Continuum (macroscopic) approaches can be used to estimate the stress ratio. For a deeper understanding, however, local conditions (at the grain/colony scale) must be taken into account. This is not to say that the externally applied stress does not play a role in the overall deformation and cavitation processes, for indeed it does influence the magnitude and sign (compressive or tensile) of the principal and mean stresses that develop within individual grains/colonies. However, the relative strength of neighboring grains/colonies is also of great importance, particularly for anisotropic materials with an hcp crystal structure such as the alpha phase of Ti-6Al-4V.

Individual grains/colonies may be characterized as hard or soft, depending on the slip systems that are activated in response to the externally applied stress. Previously, a simple approach was developed to quantify the effect of local texture on local stresses, local strains, and cavitation for cases in which the *macroscopic* loading

is compressive (e.g., uniaxial compression, forging) or shear (e.g., torsion) in nature [10, 12, 17]. In a representative volume element comprising soft and hard colonies, the former develop larger stress triaxiality and undergo larger strains than the latter. The exact partitioning of strain between neighboring hard and soft colonies depends on the ratio of their Taylor factors,  $M_h/M_s$ , in which the subscripts h and s refer to the hard and soft colonies, respectively. As the Taylor-factor ratio increases, the preferential partitioning of strain to the softer colony increases. In the subsections that follow, the approach for modeling cavity closure is briefly summarized, and model predictions are compared to the experimental observations.

#### A. Cavity-Closure Model

Cavity closure was interpreted in the context of analyses for the local stress state/strain partitioning [10, 12, 17] and the consolidation of powder compacts [18]. Previously, the consolidation model was applied successfully to predict cavity-closure behavior during reversed-torsion testing [10]. In addition to the specified initial density (or percent porosity), model inputs comprise the *local* principal stresses developed in adjacent soft and hard colonies, the effective (flow) stress of the colonies, and the strain partitioning between neighboring colonies. These quantities are determined by combining the relations for force equilibrium and the yield functions of the hard and soft colonies with self-consistent (strain-partitioning) calculations and continuum FEM analysis. In brief, the modeling steps can be summarized as follows: (i) the local principal stresses developed in the softer colony (which is assumed to control cavity-closure behavior) are determined from the force-equilibrium equations and the yield function, the latter making use of the strain-partitioning analysis to estimate the rate-dependent flow stress of the soft colony, (ii) the principal strain rates in the soft phase are determined from the principal stresses

and the densification model, and (iii) these rates are summed to obtain the densification rate. This procedure has been applied for cavitation during tension testing [17], forging [19], and torsion [12].

For the present work, the stress ratio  $\sigma_M/\sigma_e$  (in the soft colony) and the local strains (in the hard and soft colonies) as a function of the macroscopic effective strain were estimated assuming a Taylor factor ratio ( $M_h/M_s$ ) of 3 and a volume fraction of hard colonies equal to 60 pct. (Figure 7). Other inputs into the model calculations included a strain-rate sensitivity index ( $m$  value) of 0.15, and a flow-softening exponent of -0.20, consistent with the measured flow curves for compression following torsion (Figure 1). Model predictions showed that the hard colonies remained almost undeformed (Figure 7). Therefore, the overall cavitation process is essentially fully governed by the deformation of the soft colonies. In addition, during torsional prestrain, it has been shown that cavities in soft colonies have a tendency to grow under a high level of tensile stress. As shown in Figure 7, however, the stress ratio was predicted to remain *negative* throughout the subsequent compressive step of deformation, thus enabling the closure of cavities, even though the absolute magnitude of the compressive state of stress decreased as deformation proceeded.

Consolidation-model predictions of pore closure during compression following the two different torsional prestrains are compared to measurements in Figure 8. The two solid lines correspond to model predictions in which the absolute magnitude of the stress ratio decreased with deformation (i.e., the stress ratio became less *compressive*) per the results shown in Figure 7. Not unexpectedly, the rate of cavity closure was thus predicted to decrease with increasing deformation due to the decrease in mean compressive stress and the increase in density. This behavior has important industrial implications, for the majority of cavity closure may take place

only in the early stages of compression. In fact, in some cases, there may be a point after which additional deformation may actually lead to cavity initiation and growth. The model predictions in Figure 8 also show a hypothetical upper bound on cavity closure (viz., the broken line for the torsional prestrain of 1.78), which was obtained by assuming that the stress ratio remained constant at a value equal to that at the beginning of the compressive deformation.

The cavity-closure model predictions are also compared to measurements in Figure 8. Despite the lack of several measurements within the compressive strain range between 0 and 0.29 (height reduction between 0 and 25 pct.), the model does appear to provide first-order agreement with the observations.

#### *B. Comparison of Cavity Closure in Compression and Reversed Torsion*

The model for consolidation of porous media can also be used to explain at least qualitatively the source of the difference in cavity shrinkage rates for reversed torsion versus compression following forward torsion. The slower rate of cavity shrinkage during reversed torsion (Figures 4, 6) can be ascribed partially or wholly to three factors (i) cavity orientation with respect to the torsion axis, (ii) the loss of strength differences between neighboring colonies because globularization leads to a more homogeneous microstructure, and (iii) flow softening.

With regard to the first factor, because cavities developed in torsion tend to be elongated, not all of them can be closed in reversed torsion. Only those which are oriented favorably with respect to the torsion axis, i.e., at a finite angle, can be closed. In particular, cavities oriented at an angle of  $45^\circ$  with the torsion axis experience a high rate of closure, while those that are parallel to the torsion axis remain intact. The rate of closure decreases as the cavity orientation decreases from  $45^\circ$  to zero degrees. According to the powder-consolidation model, if all of the cavities were oriented at an

angle of 45°, reversed torsion would have a cavity-closure rate similar to that of the compression.

When the microstructure globularizes *at large strains* and there is no difference in the strength of the material that surrounds a cavity, reversed torsion becomes ineffective in closure because the material behaves locally as a continuum and the mean stress is zero. By contrast, even after a fully globularized microstructure is realized, compression following torsion still promotes cavity closure because the local stress ratio is negative (compressive state of stress).

The third factor, which can contribute to the observed difference in cavity closure in reversed torsion and compression, is flow softening. Reheating and soaking of specimens machined from torsion samples led to a high flow-softening rate ( $\sim 0.22$ ) during compression as opposed to a zero flow-softening rate during reversed torsion following immediately after forward torsion (Figure 1). As has been discussed previously [17], the absolute value of the stress ratio  $\sigma_M/\sigma_e$  is higher for a material that undergoes flow softening compared to one which has a zero or positive strain-hardening exponent. Thus, the stress ratio during the compression tests is more negative compared to that in reversed torsion, and therefore the cavity *closure* rate is higher.

### C. Engineering Approach to Cavity Closure

During forward torsional deformation, cavity initiation and growth takes place. These cavities shrink during subsequent compression or reversed torsional deformation. An approximate analysis of the initial and final cavity radii  $r_o$  and  $r_f$  (i.e., the radii after forward torsion versus those after reversed torsion or compression) was performed to estimate the cavity-*closure* rate during the strain-path change. For this purpose, attention was focused on two specific cases (Figure 9): (i) forward

torsion (FT) to a surface effective strain of 0.99 (twist angle = 125°) followed by reversed torsion (RT) to a surface effective strain of 0.25 (twist angle = 31.3°) and (ii) forward torsion (FT) to a surface effective strain of 0.99 (twist angle = 125°) followed by compression to an effective strain of 0.29 (25 pct. height reduction). Because it is not possible to measure the initial and final radii of specific cavities, a statistical approach was taken for the measurements in Figure 9. In particular, individual data points in the figure correspond to the average size ( $r_o$ ) of the 5 largest cavities, second 5 largest cavities, etc. after FT in comparison to the size ( $r_f$ ) of the 5 largest, second 5 largest, etc. cavities after FT + RT or FT + compression.

The rates of cavity closure during RT or compression (Figure 9) were quantified by applying the closure analog of the classical cavity-growth equation [5, 9], i.e.,  $r_f = r_o \exp(\eta \bar{\epsilon})$ , in which  $r_f$  and  $r_o$  denote the final and initial cavity sizes (as described above),  $\eta$  is the rate of cavity-growth or, in the present case, shrinkage, and  $\bar{\epsilon}$  is the macroscopic effective strain. The continuous lines shown in Figure 9 represent the best fit of this equation (i.e., straight lines passing through the origin with slopes  $dr_f/dr_o$  equal to  $\exp(\eta \bar{\epsilon})$ ), thus providing the value of the cavity-*shrinkage* rate  $\eta$ , viz., -4.0 for compression and -1.5 for torsion, for a strain  $\bar{\epsilon} = 0.29$  and  $\bar{\epsilon} = 0.25$  respectively. It should be borne in mind that these values of  $\eta$  are for relatively small reversed strains ( $\bar{\epsilon} \sim 0.3$ ) and pertain to the regime of rapid closure. Smaller values of  $\eta$  would be expected at larger strains as closure slows down. In other words, if the same approach were applied for higher strains, the magnitudes of  $\eta$  would be lower. From a practical, industrial perspective, this behavior implies that there is little benefit in applying extremely high strains to reduce/minimize cavitation,

because the majority of cavity shrinkage occurs early with little additional closure at large strains.

## V. SUMMARY

The effect of strain path on deformation and cavitation during hot working of Ti-6Al-4V with a colony-alpha microstructure was quantified via torsion-compression and torsion-reversed torsion experiments at 815°C. It was found that the rate of closure of cavities formed during forward torsion depended on the subsequent deformation mode. Compression was much more effective than reversed torsion in bringing about cavity closure. The cavity-closure observations were successfully quantified using a model previously developed to treat the consolidation of powder compacts. In addition, a cavity-closure rate for each case was determined; for effective strains between 0 and ~0.3, the cavity-closure rate in compression is more than twice that for reversed torsion. At larger strains, the closure rate decreases, suggesting the limited effectiveness of large strains in healing cavitation damage.

**Acknowledgements-** This work was conducted as part of the in-house research activities of the Metals Processing Group of the Air Force Research Laboratory's Material and Manufacturing Directorate. The support and encouragement of the Laboratory management and the Air Force Office of Scientific Research (Capt. Brett Conner, program manager) are gratefully acknowledged. One of the authors (PDN) was supported under Air Force contract FA8650-04-D-5235. The assistance of Messrs. R.L. Goetz and P.N. Fagin in conducting the FEM analysis and mechanical testing, respectively, is highly appreciated.

## REFERENCES

1. C.C. Bampton and J.W. Edington: *J. Eng. Mater. Tech.*, 1983, vol. 105, pp. 55-60.
2. M.B. Taylor, H.M. Zbib, and M.A. Khaleel: *Int. J. Plasticity*, 2002, vol. 18, pp. 415-442.
3. M.M.I. Ahmed and T.G. Langdon: *Metall. Trans. A*, 1977, vol. 8A, pp. 1832-1833.
4. M.J. Stowell: in *Superplastic Forming of Structural Alloys*, N.E. Paton and C.H. Hamilton, eds., TMS-AIME, Warrendale, PA, 1982, pp. 321-26.
5. A.H. Chokshi: *J. Mater. Sci.*, 1986, vol. 21, pp. 2073-2080.

6. R. Verma, P.A. Friedman, A.K. Ghosh, S. Kim, and C. Kim: *Metall. Mater. Trans. A*, 1996, vol. 27A, pp. 1889-1898.
7. H. Agarwal, A.M. Gokhale, S. Graham, and M.F. Horstemeyer: *Mater. Sci. Eng. A*, 2003, vol. A341, pp. 35-42.
8. D.H. Bae, A.K. Ghosh, and J.R. Bradley: *Metall. Mater. Trans. A*, 2003, vol. 34A, pp. 2449-2463.
9. J. Pilling and N. Ridley: *Acta Metall.*, 1986, vol. 34, pp. 669-679.
10. P.D. Nicolaou and S.L. Semiatin: *Metall. Mater. Trans. A*, 2006, vol. 37A, pp. 3697-3705.
11. N. Ridley, P.S. Bate, B. Zhang, *Mater. Sci. Eng. A*, 2007, vol. A463, pp. 224-230.
12. P.D. Nicolaou, J.D. Miller, and S.L. Semiatin: *Metall. Mater. Trans. A*, 2005, vol. 36A, pp. 3461-3469.
13. P.D. Nicolaou and S.L. Semiatin: *Metall. Mater. Trans. A*, 2007, vol. 38A, in press.
14. S.L. Semiatin, R.L. Goetz, E.B. Shell, V. Seetharaman, and A.K. Ghosh: *Metall. Mater. Trans. A*, 1999, vol. 30A, pp. 1411-1424.
15. S.L. Semiatin and J.J. Jonas: in *Handbook of Workability and Process Design*, G.E. Dieter, H.A. Kuhn, and S.L. Semiatin, eds., Chapter 7, ASM International, Materials Park, OH, 2003, pp. 86-121.
16. S.L. Semiatin and T.R. Bieler: *Acta Mater.*, 2001, vol. 49, pp. 3565-3573.
17. T.R. Bieler, P.D. Nicolaou, and S.L. Semiatin: *Metall. Mater. Trans. A*, 2005, vol. 36A, pp. 129-140.
18. D.P. DeLo, R.E. Dutton, S.L. Semiatin, and H.R. Piehler: *Acta Mater.*, 1999, vol. 47, pp. 3159-3167.
19. P.D. Nicolaou and S.L. Semiatin: *Metall. Mater. Trans. A*, 2005, vol. 36A, pp. 1567-1574.

## Figure Captions

- Figure 1. Effective stress-strain curves for torsion followed by reversed torsion or compression. The initial (forward) torsional deformation consisted of a twist of (a)  $125^\circ$  or (b)  $225^\circ$ , corresponding to surface effective strains of 0.99 and 1.78, respectively.
- Figure 2. FEM predictions of the variation of principal and mean stresses with stroke during compression following torsion.
- Figure 3. Micrographs from the r-z plane showing the extent of cavitation after (i) forward torsion, (ii) reversed torsion, and (iii) compression. The initial (forward) torsional twist was (a)  $125^\circ$  or (b)  $225^\circ$ .
- Figure 4. Cavity area fraction as a function of the macroscopic effective strain for reversed torsion and compression.
- Figure 5. Variation of the equivalent cavity radii for the 30 largest cavities within forward torsion, reversed-torsion, and compression specimens. The initial (forward) torsional twist was (a)  $125^\circ$  or (b)  $225^\circ$ .
- Figure 6. Reduction in equivalent cavity radius as a function of the initial cavity size for reversed torsion and compression.
- Figure 7. Local effective strain for hard and soft colonies and the stress ratio in soft colonies as a function of macroscopic effective strain during compression.
- Figure 8. Model predictions of cavity fraction as a function of macroscopic effective strain during compression based on the (actual) increasing stress ratio (solid lines) or an assumed stress ratio equal to that at the beginning of compression (broken line). The predictions are compared to experimental results (data points).

Figure 9. Measured final-versus-initial cavity radii for reversed torsion tests and compression used to determine the rate of cavity closure.

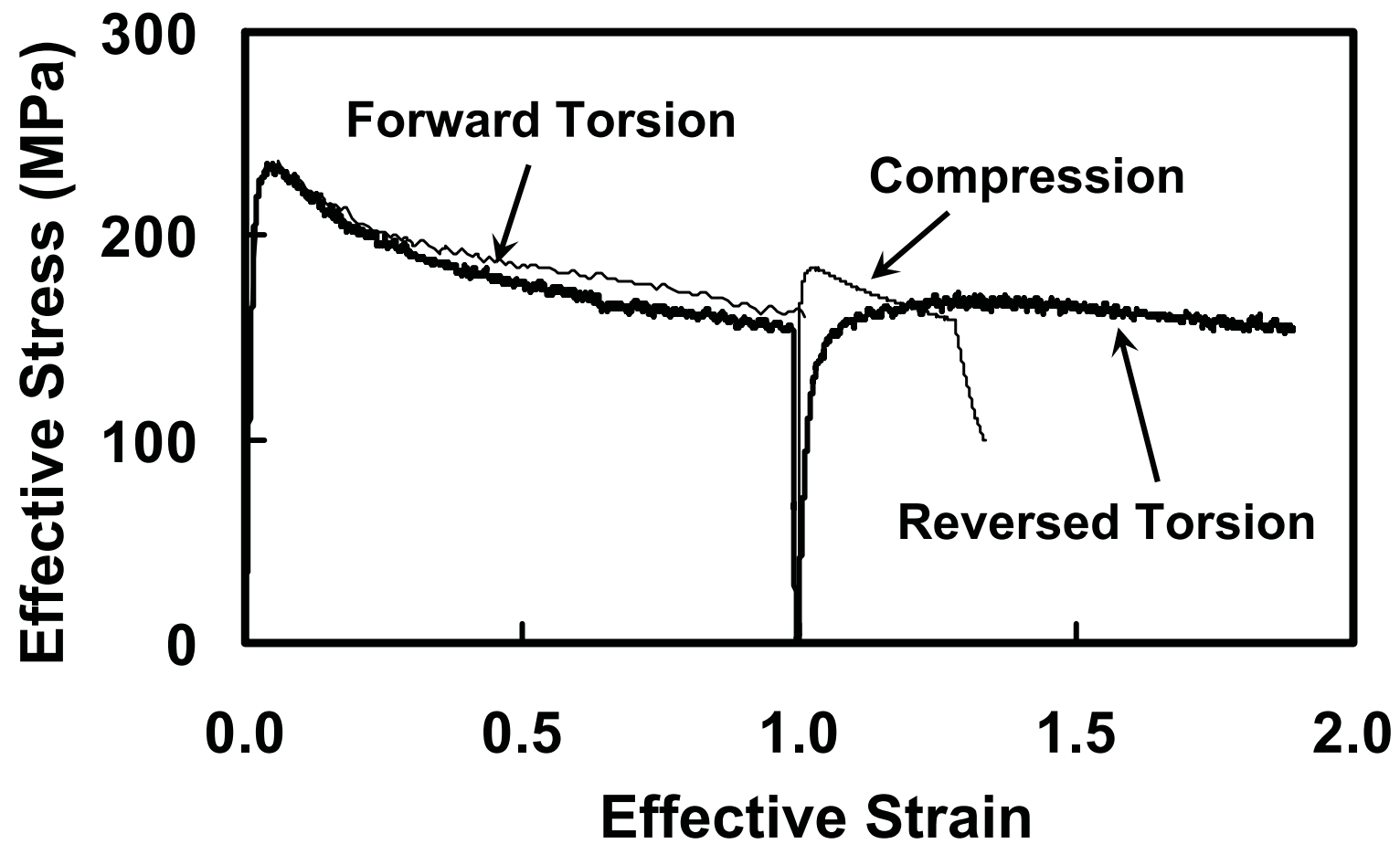


FIGURE 1a

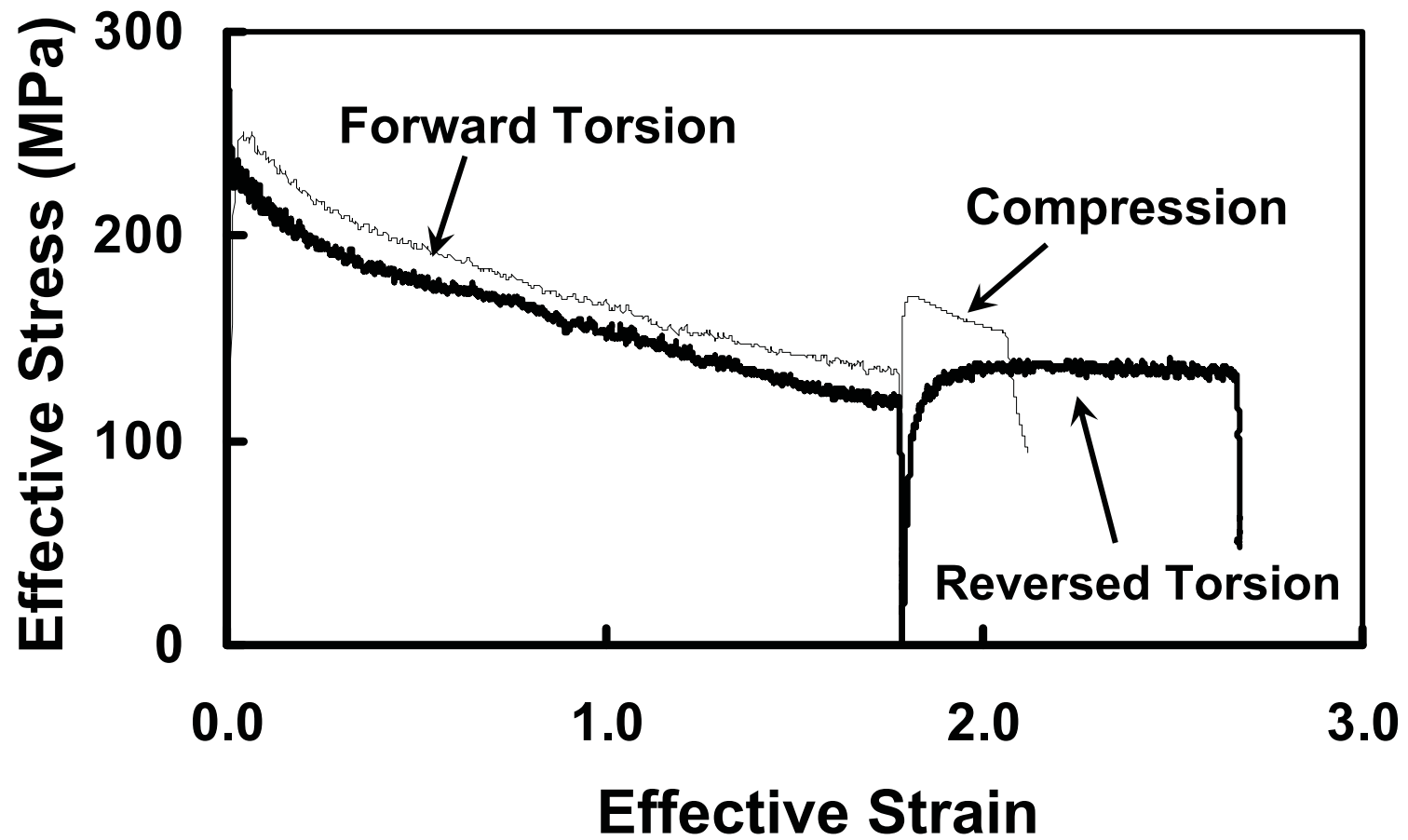


FIGURE 1b

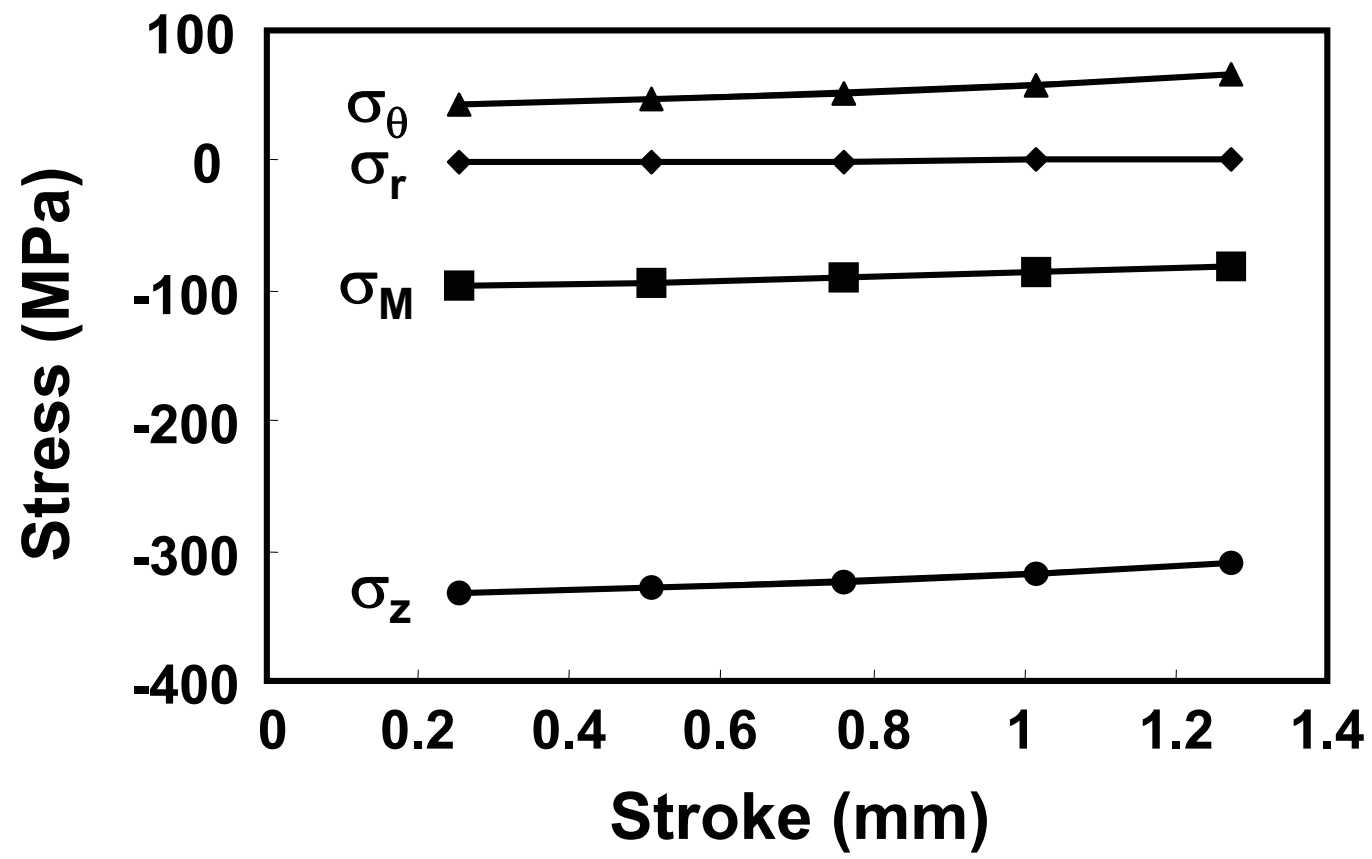
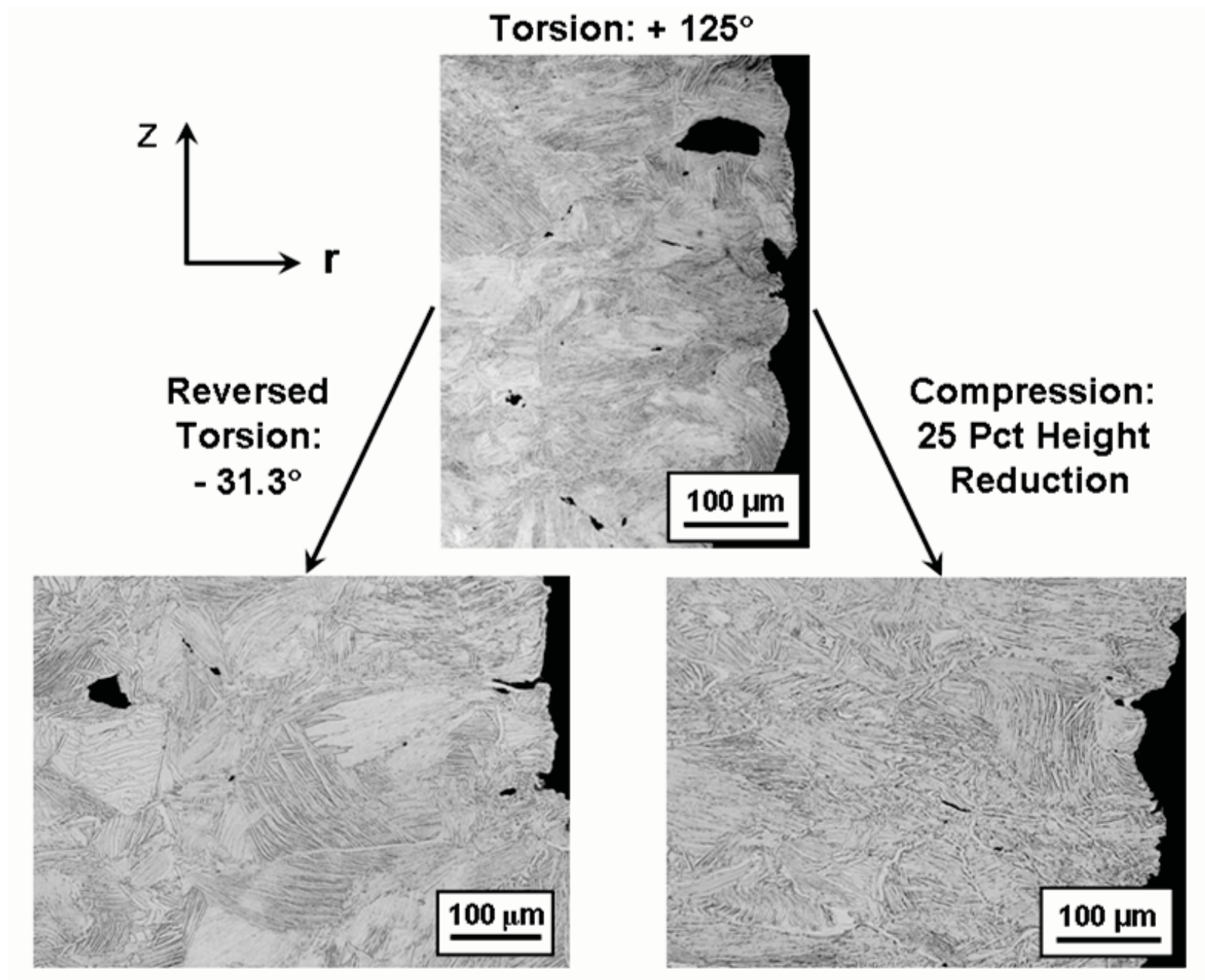
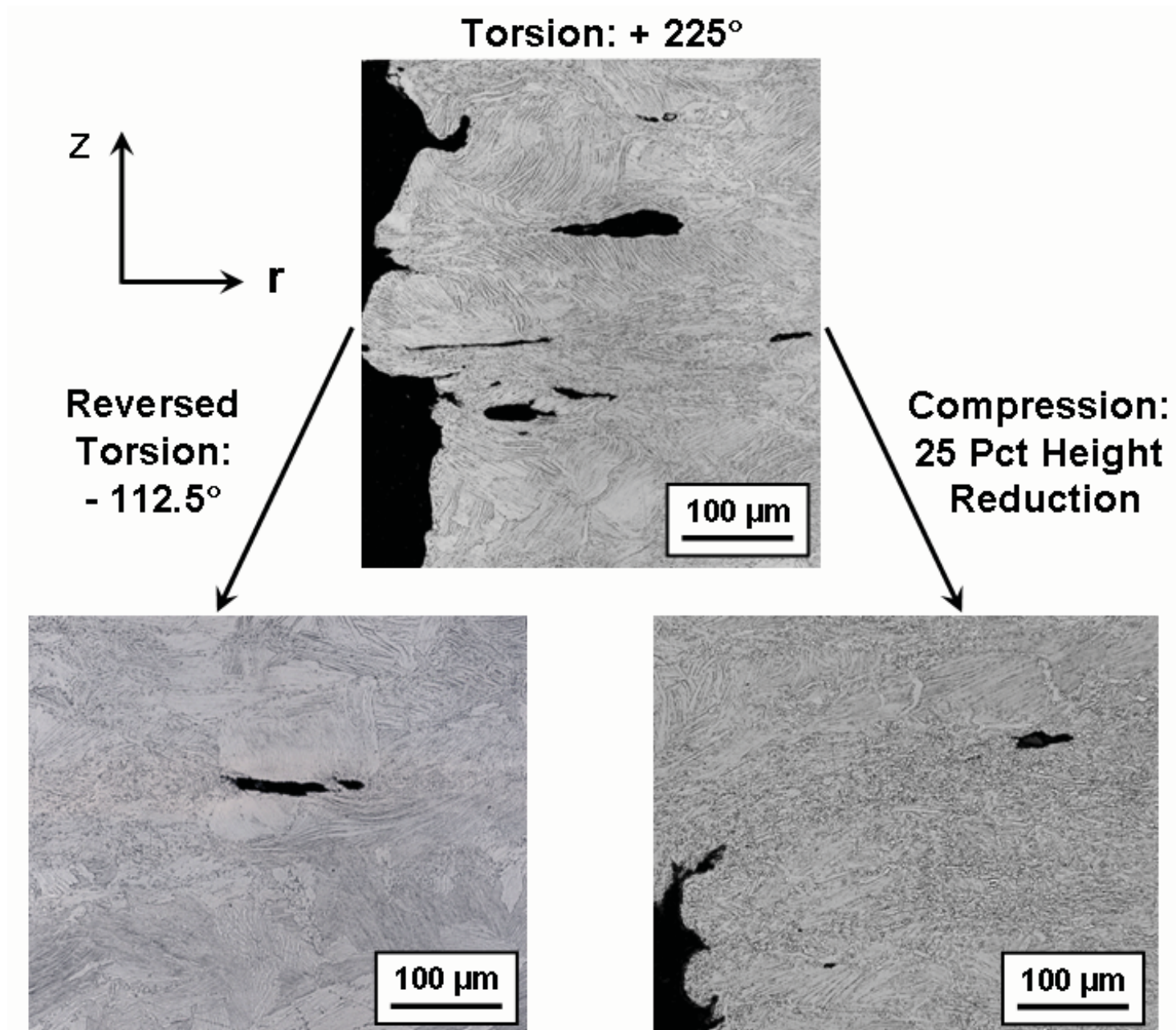


FIGURE 2



**FIGURE 3a**



**FIGURE 3b**

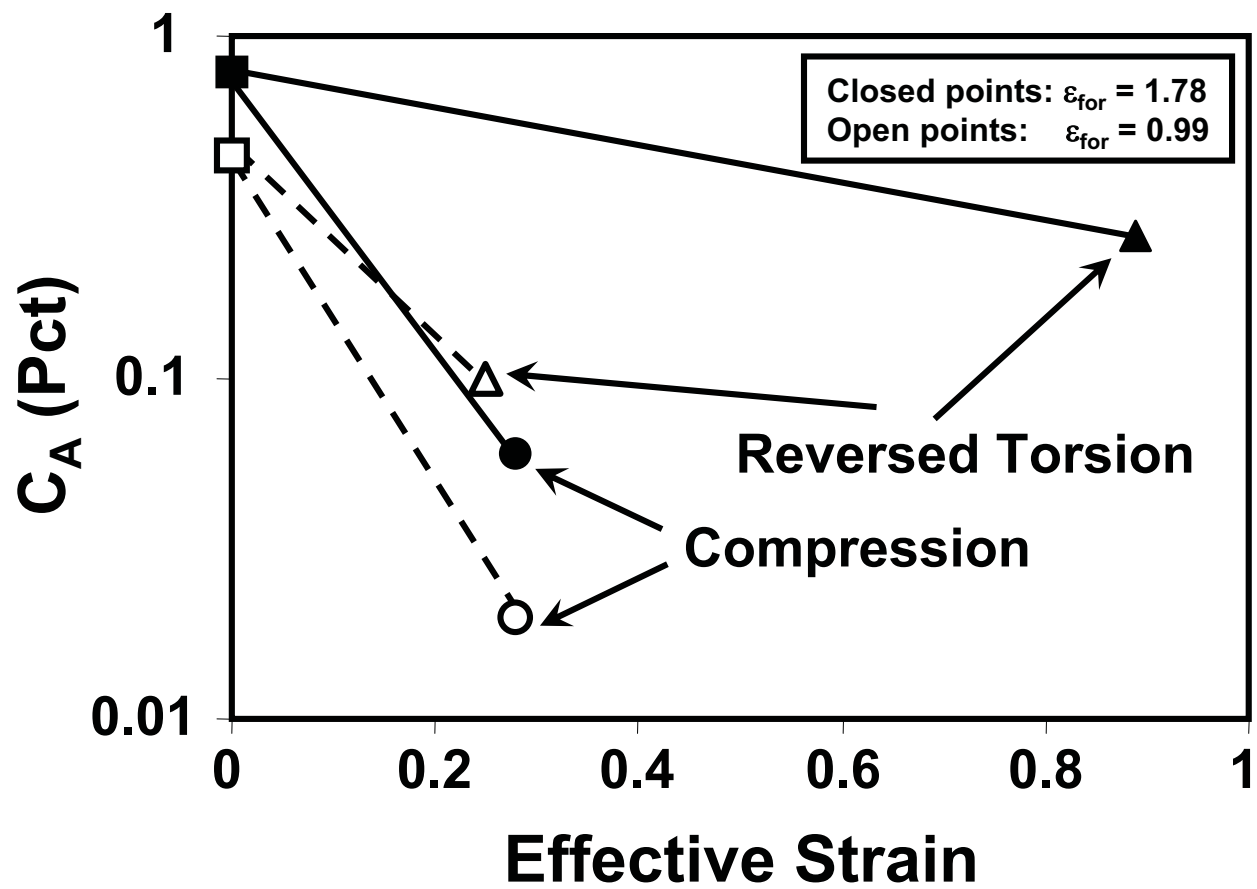


FIGURE 4

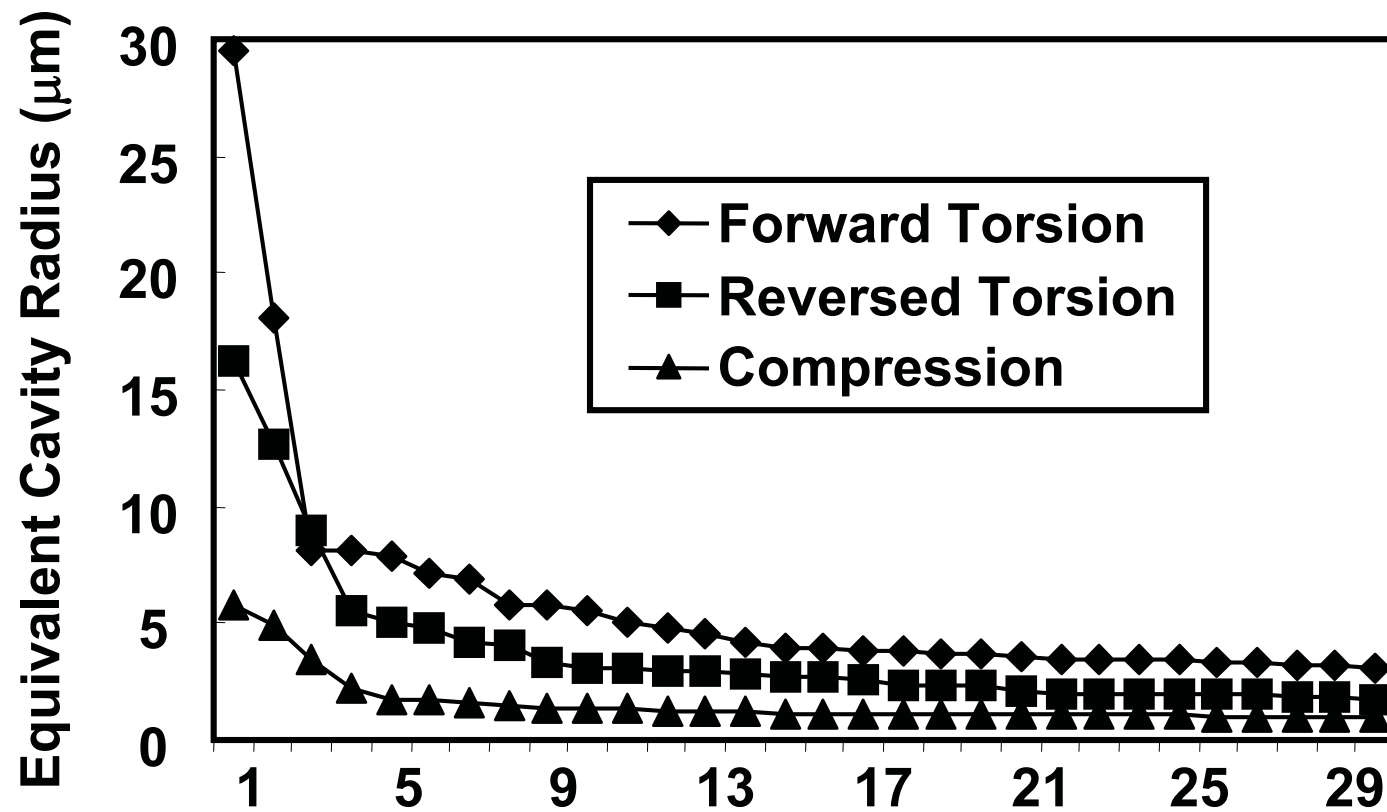


FIGURE 5a

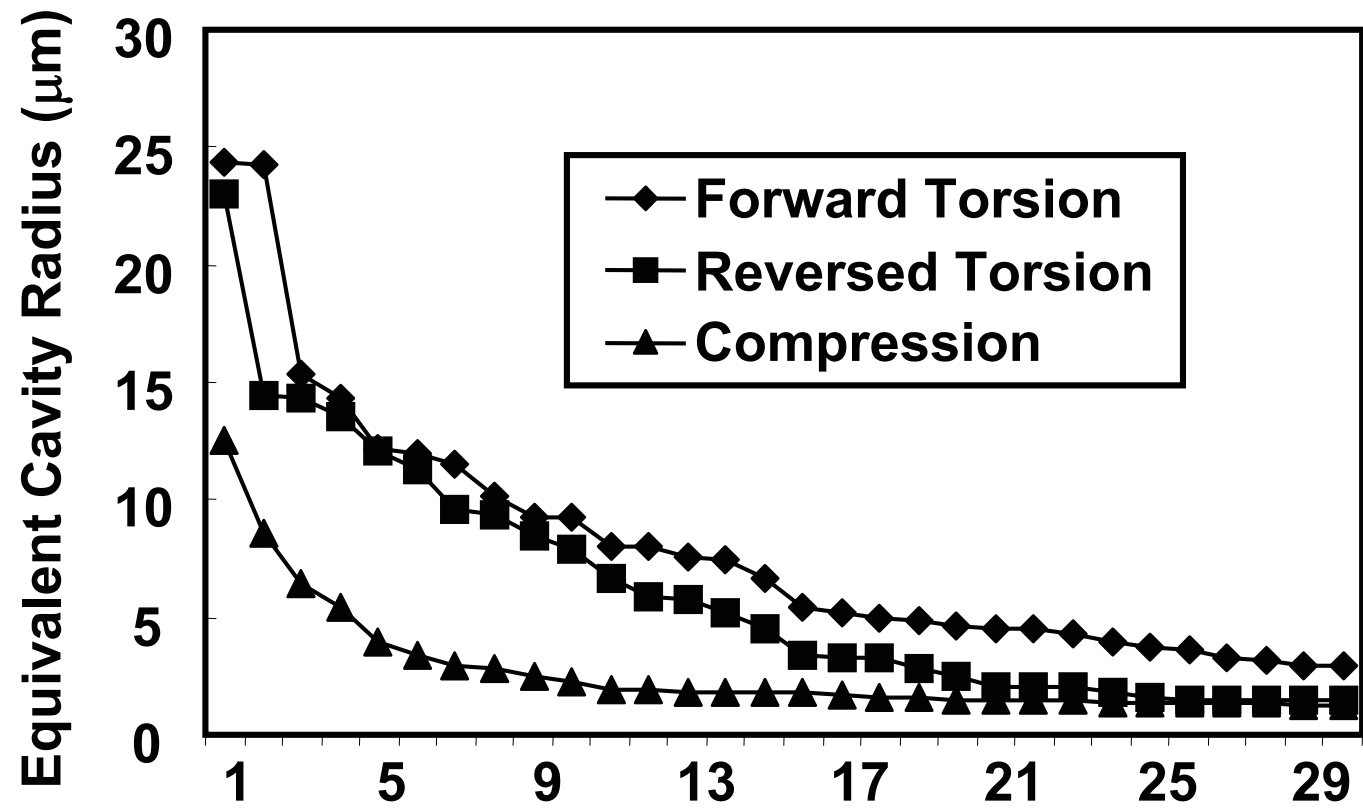
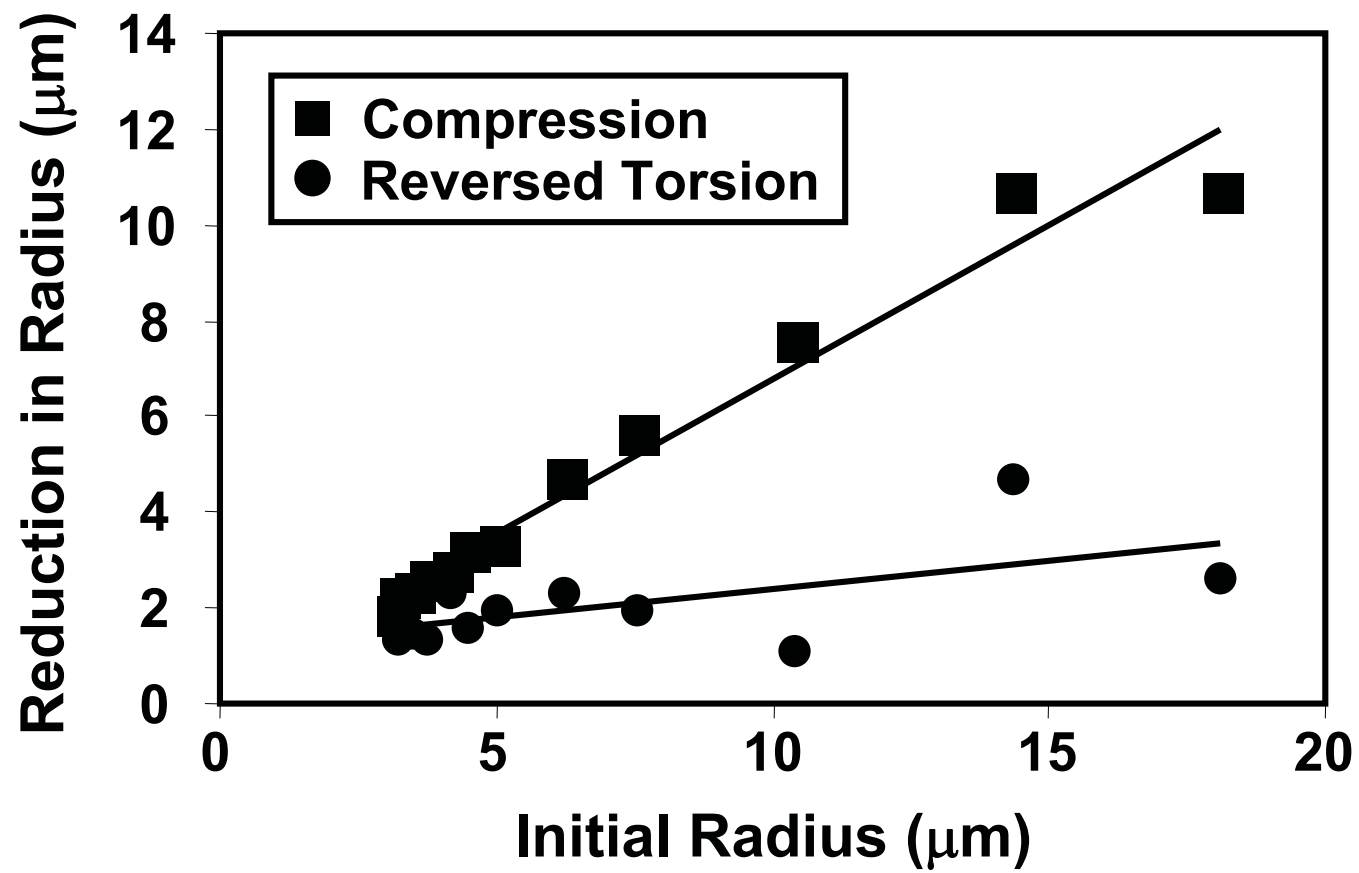


FIGURE 5b



**FIGURE 6**

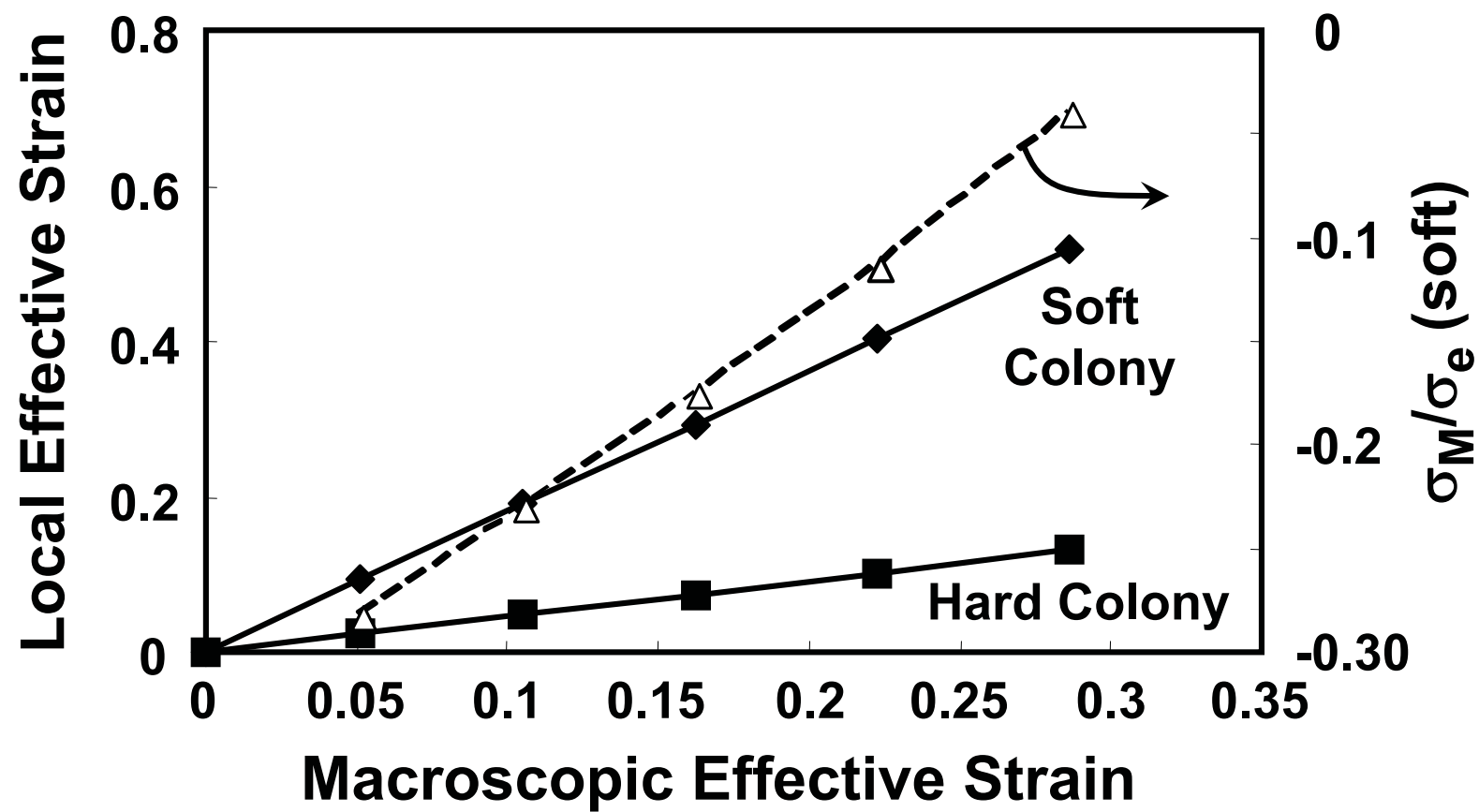


FIGURE 7

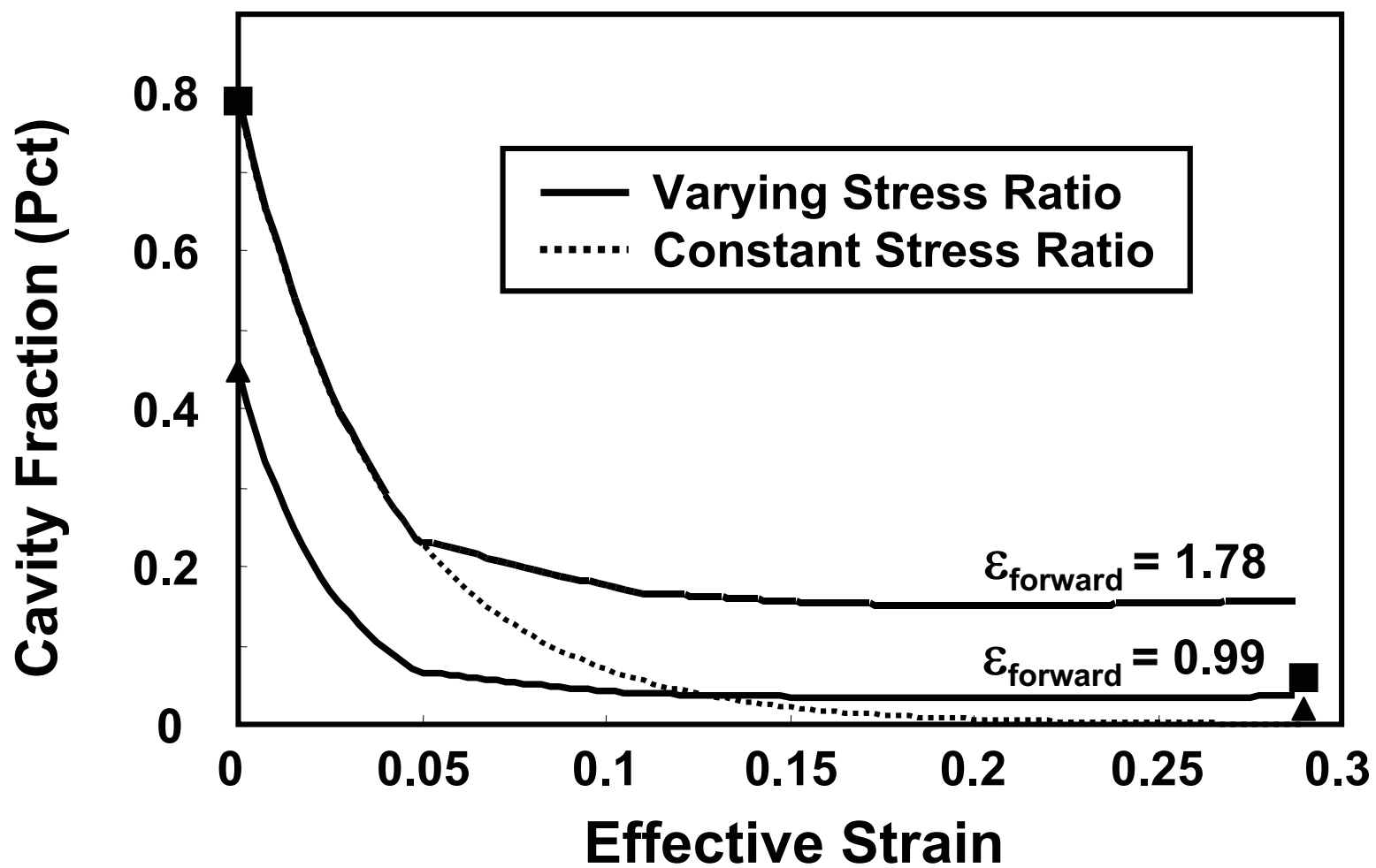


FIGURE 8

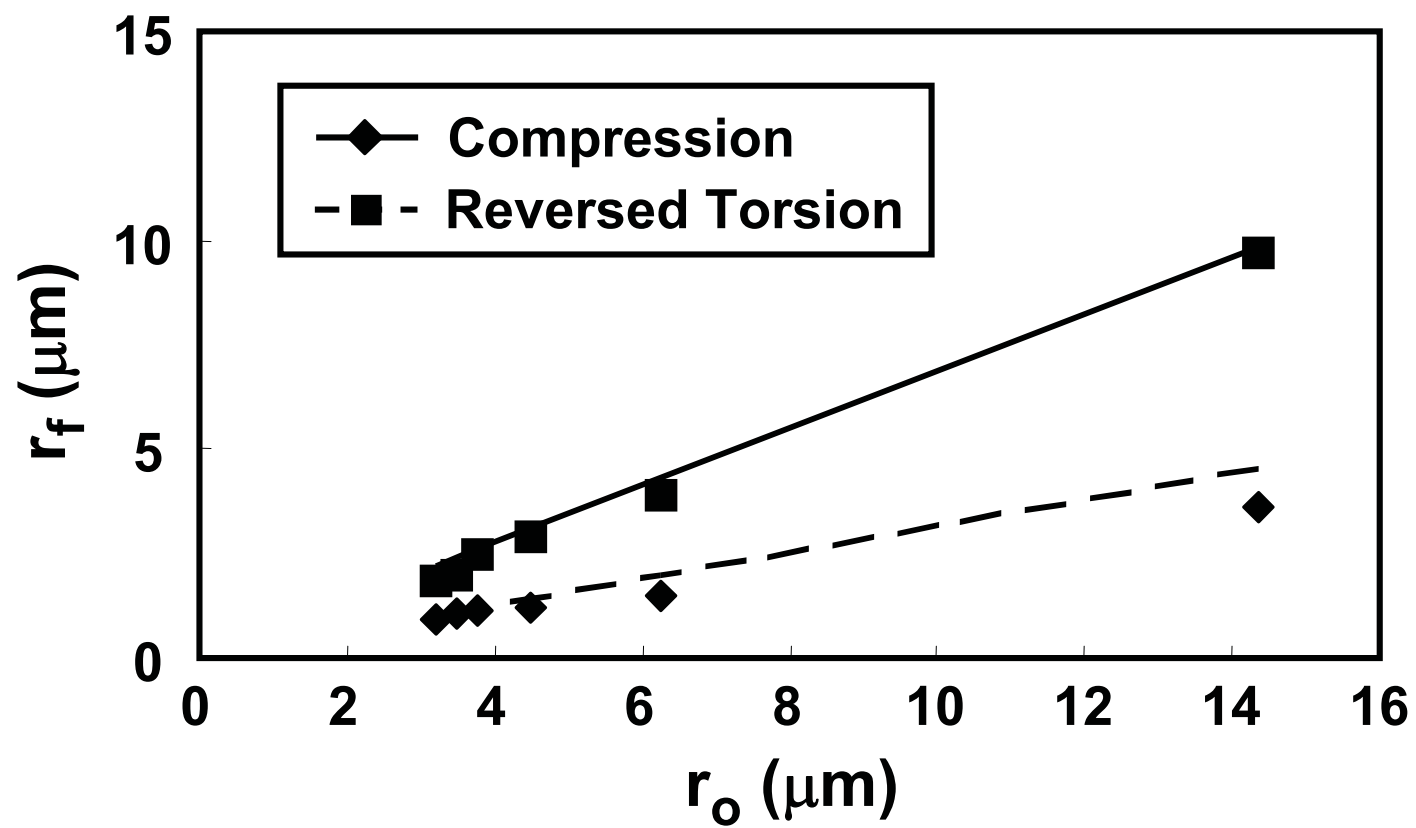


FIGURE 9